Title

Analysis of chemical stress and the propensity for cracking during the vertical Bridgman growth of BaBrCl:Eu

Authors

Zhang, Chang
Gao, Bing
Tremsin, Anton S
et al.

Publication Date

2020-09-01

DOI

10.1016/j.jcrysgro.2020.125794

Peer reviewed

Analysis of chemical stress and the propensity for cracking during the vertical Bridgman growth of BaBrCl:Eu

Chang Zhang[a], Bing Gao[b], Anton S. Tremsin[c], Didier Perrodin[d], Tetiana Shalapska[d], Edith D. Bourret[d], Drew R. Onken[d,e], Sven C. Vogel[f], Jeffrey J. Derby[a,*]

[a]*Department of Chemical Engineering and Materials Science, University of Minnesota, Minneapolis, MN 55455, USA*
[b]*Institute of Technological Sciences, Wuhan University, Wuhan City, China 430072*
[c]*Space Sciences Laboratory, University of California at Berkeley, Berkeley, CA 94720, USA*
[d]*Lawrence Berkeley National Laboratory, Berkeley, CA 94720, USA*
[e]*Department of Physics, Wake Forest University, Winston-Salem, NC 27109, USA*
[f]*Materials Science & Technology Division, Los Alamos National Laboratory, Los Alamos, NM 87545, USA*

Abstract

Computational models are employed to analyze residual chemical stresses arising from compositional variations in europium-doped BaBrCl crystals grown by the vertical Bridgman method. We find that significant chemical stress is produced by radial segregation of Eu in this system. In particular, the distribution of normal stresses is set by the radial concentration gradient, whose changing sign produces surface states in tension or compression. Crack opening from surface flaws will be promoted or suppressed by tensile or compressive surface stresses, respectively. Thus, crystal growth processing strategies that change the radial dopant concentration gradients are posited to affect the propensity for cracking. For this system, surface stresses are changed from states of tension to compression when the growth rate is increased, thus improving the chances to avoid cracking—a strategy that defies classical wisdom that dictates slower growth to improve outcomes. Similar strategies affecting segregation may prove beneficial to tailor chemical stress fields to reduce cracking in other crystal growth systems.

Keywords: A1. Computer simulation; A1. Chemical stress; A1. Convection; A1. Segregation; A2. Bridgman technique; B2. Scintillator materials

1. Introduction and Background

Barium bromochloride, doped with europium (BaBrCl:Eu), is a good scintillator crystal for X-ray and gamma-ray detection [1–3]. In previous studies, we have applied energy-resolved neutron radiography to image, in real time and *in situ,* the vertical gradient freeze growth of BaBrCl:Eu [4, 5]. Following this work, we employed computational models to analyze the mechanisms that were responsible for the observed interface shape evolution and solute segregation in this experiment [6]. In related work on assessing the challenges for crystal growth of BaBrCl:Eu, Bourret *et al.* [2, 7] identified cracking as a potential problem that could affect the production of this material. In fact, halide scintillators are unusually prone to cracking and resultant yield losses [8].

Cracking is a complicated phenomenon that is neither well understood nor well studied for many crystal growth systems. Brice [9] presented one of the earliest of analyses of cracking of brittle, Czochralski-grown

*Corresponding author:
Email address: derby@umn.edu (Jeffrey J. Derby)

crystals by thermal effects and derived scaling laws meant to keep radial temperature gradients low enough to avoid a postulated, instantaneous "breaking strain." Subsequent analyses of cracking in crystal growth systems have generally adopted this idea that cracking arises when a critical strain or stress level set by the temperature field is exceeded; see, e.g., [10–13]. Stress and strain arising from thermal effects is significant in virtually all melt growth systems due to temperature gradients that occur during growth and over the cool-down period.

Instantaneous thermal stresses may promote cracking, as posited by the prior studies referred to above [9–13], and the important role of such thermal stresses on cracking has been documented in many prior experimental studies [14–23]. However, a solid can also experience *residual* stresses remaining in the material after the original cause has been removed [24] that can delay cracking to during unloading or processing. In high-temperature crystal growth systems, residual stress can result from plastic deformation, arising from dislocation movement and multiplication, that is driven by thermal effects and frozen-in after growth. The role of thermal stresses on dislocation generation and multiplication has been extensively studied in melt crystal growth, originally with the aim to understand dislocation levels in semiconductor single crystals [25–28]. Gao, Kakimoto, and co-workers have extended these ideas to represent dislocation motion and generation in preferred slip planes over three spatial dimensions to analyze the generation of residual stress in silicon and sapphire crystals [13, 29–32].

Another source of residual stress, of particular interest here, is that arising from strains introduced by compositional variations in a single crystal, a phenomenon referred to as chemical stress. Strain introduced by dopants has been discussed in many previous reports on the cracking of brittle, single crystals. For example, Cockayne *et al.* [15], Brice [9], and Eakins *et al.* [16] comment on strain arising from compositional effects due to growth striations and facets, over which different segregation occurs compared to non-facetted interfaces that are growing steadily. Chemical stress arising from spatial compositional inhomogeneities was identified as the dominant factor in the cracking of bulk single crystals by Bachmann *et al.* [33] and Dutta and Ostrogorsky [34] for quaternary and ternary III-V alloys. Kimura *et al.* [35] found that Czochralski-grown $Gd_3(Ga_{1-x}Al_x)_5O_{12}$ single crystals were less likely to crack under certain compositional ranges due to the effects of composition on strain. Finally, Sangeeta *et al.* [36, 37] identified non-stocihiometric compositional effects as strongly influencing cracking during the Czochralski growth molybdate crystals of lead, cadmium, and zinc.

While intuitively satisfying, the notion of a "breaking strain" is a rather coarse representation of the physical mechanisms that explain how crack propagation occurs. Griffith's classical analysis of brittle fracture [38] asserts that the propagation of an existing crack occurs when the elastic energy associated with the release of strain stored in a stressed material is greater than the additional energy that arises with extending

the crack surfaces. This idea requires two conditions for cracking, a sufficiently high state of stress and strain coupled with a small, existing crack. This micro-crack may exist due to surface damage or be associated with an imperfection within the bulk of a material, such as an embedded foreign particle or a second phase.

The initiation of a crack from surface flaws and bulk imperfections has been reported in previous experimental studies of cracking during crystal growth. Ballman *et al.* [14] discussed the growth of barium-sodium niobate crystals by the Czochralski method and posited that lattice distortion associated with a ferroelectric transition augmented thermal strains to propagate cracks nucleated on the surface of the crystal and from interior flaws. Cockayne *et al.* [15] reported on factors that influence cracking in Czochralski-grown yttrium orthoaluminate crystals. They identified extrinsic factors, such as cooling rate and crystal size, that set the strain levels in the crystal and also discuss intrinsic factors, such as surface flaws and voids and second phases in the bulk, that could serve to initiate a crack. Eakins *et al.* [16] considered cracking during the Czochralski growth of neodymium-doped yttrium aluminum garnet, focussing on the role of voids and neodymium-rich particles on the initiation of cracks, which then propagated under thermal stress.

Returning to the material of interest here, Bourret *et al.* [2, 3] found that $BaBr_2$ and $BaCl_2$ form a solid solution in the whole range of composition and that BaBrCl crystallizes in an orthorhombic, three-dimensional $PbCl_2$ structure-type with a Pnma space group [39, 40]. They were subsequently able to successfully grow BaBrCl single crystals doped at 5% europium using both a vertical Bridgman-Stockbarger technique and a pressurized Czochralski method. Cracking was noted as a problem, particulalry for increased levels of Eu doping, but improvements were observed using a growth configuration that reduced thermal gradients and by slower cooling after growth [7]. For all mixed halide scintillators grown by Bourret *et al.* [2], residual moisture and impurities were also noted to increase the likelihood of cracking.

In addition to the real-time imaging of crystal growth described in [4–6], Tremsin *et al.* [4, 5, 41] applied neutron transmission to perform tomographic interrogation of the grown crystals. Their results indicated a strong correlation between Eu distribution and cracking and that cracks originated from clusters where Eu concentration gradients were large. Later, Onken *et al.* [42] used neutron diffraction to measure the lattice structure of undoped and 5% Eu-doped BaBrCl crystals at elevated temperatures. They reported anisotropic thermal expansion that produces thermal strain and found significant chemical strain caused by the presence of europium dopant atoms substituting at the barium site. The chemical strain, defined as difference in lattice parameters between doped and undoped material relative to the undoped material, peaked at a temperature of 673 K, which correlated to experimental observations of crack formation in that temperature range. They posited that the additive effect of chemical strain to thermal strain led to crack formation in BaBrCl:Eu.

These findings motivate the analysis presented here, in which we carry out calculations for the segregation

and associated chemical stress distributions in BaBrCl:Eu crystals grown by a vertical Bridgman method. We are particularly interested in identifying the relations among growth conditions and segregation behavior, the resulting chemical stress distributions, and their effect on cracking. While the effects of thermal stresses on cracking are widely appreciated, we believe that the following analysis is one of the very first to analyze the role of chemical residual stresses on cracking.

2. Analysis Methods

We employ two analysis tools in this study. The first is a model for crystal growth and europium segregation in a vertical Bridgman-Stockbarger system that is representative of that experimentally employed by Bourret *et al.* [2, 3, 7], and the second is a solid mechanics model that computes residual stresses arising from nonuniform dopant distribution. Both models apply idealizations to ease computational burden and are not meant to be quantitatively predictive, rather they are applied to clarify the phenomenological linking of segregation to chemically-induced stress patterns.

The idealized crystal growth system is shown schematically in Figure 1(a) and consists of a cylindrical ampoule with an inner radius of 6.5 mm and a wall thickness is 0.65 mm, aligned with the direction of gravity and made of fused quartz. The ampoule contains regions of crystal and melt, within which a dopant is distributed. A linear temperature profile with a vertically stabilizing axial gradient of 19.3 K/cm is imposed along the outer ampoule wall and swept upwards at velocity V_g, which we subsequently refer to as the growth rate, driving directional solidification from the bottom to top.

The crystal growth model is two dimensional and axisymmetric, whereby a cylindrical coordinate system consisting of radial, axial, and azimuthal components, (r, z, θ), is employed and all quantities assumed independent of θ. The governing equations are defined over three subdomains, melt, crystal, and ampoule, to describe the time-dependent, continuum transport of heat and species, as well as melt flow and solidification. The detailed model will not be discussed here but is the same as applied in our previous works that model Bridgman growth systems [43–47].

Coupled, nonlinear partial differential equations in the model are solved by the Galerkin finite element method, using a mesh that comprises 7,623 biquadratic elements that represents a total of 109,546 equations; see Figure 1(b). An implicit, trapezoid method is employed to integrate the system in time, and the Newton-Raphson method is used to linearize these nonlinear equations and solve them iteratively at each time step. The linear equations of each Newton iteration are solved directly using Gaussian elimination. The solid-liquid interface lies along the melting-point isotherm, whose position and shape are not known *a priori,* and a deforming mesh is used to represent this moving boundary. The mesh deforms according to an elliptic mesh

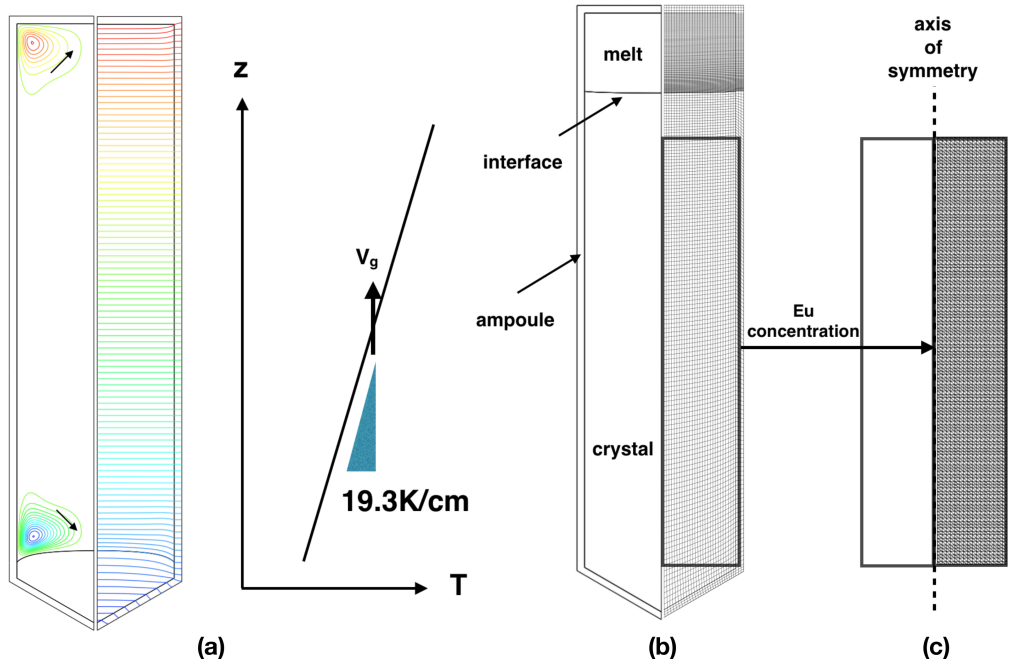

Figure 1: (a) Transient growth in a vertical Bridgman system is modeled using an upward movement of a linear temperature profile at a constant velocity, V_g. The steady state used as the initial condition for all transient simulations is shown on the left, with streamlines plotted in the left half and arrows denoting the direction of flow; streamfunction maximum and minimum are $\Psi_{max} = 1.46 \times 10^{-4}$ (counterclockwise as shown above) and $\Psi_{min} = -2.46 \times 10^{-4}$ (clockwise as shown above). Isotherms are plotted in the right half at a constant increment of $\Delta T = 0.92K$ around the melting point to show the temperature field. (b) The domains and finite element mesh are shown for the crystal growth model. Concentration data within the indicated rectangle is provided to the stress model. (c) Mesh employed for the finite-element stress model.

generation method, with node locations parameterized by a pair of elliptic partial differential equations. The finite-element code Cats2D [48] is employed for these calculations.

The dopant compositional field that has resulted due to growth and segregation is provided as input to the separate, solid mechanics model to compute residual chemical stress, as indicated schematically in Figures 1(b) and (c). Even with an axisymmetric europium distribution in the crystal, the underlying crystallographic structure and anisotropic mechanical properties produce a three-dimensional stress field; see, e.g., [13, 49]. To avoid the effort and complexity of three-dimensional calculations, we apply the approach of Lambropoulos [50] to approximate elastic stresses using a simpler, two-dimensional representation.

Lambropoulos [50] compared elastic stress solutions computed by several two-dimensional approaches to the fully three-dimensional states computed with elastic anisotropy. He considered cylindrical crystals growing in the $\langle 1\,0\,0 \rangle$ and $\langle 1\,1\,1 \rangle$ directions, under temperature distributions representative of those arising during melt crystal growth. For these systems, he found that assuming purely isotropic behavior led to an under-prediction of stress levels by approximately a factor of two.

However, Lambropoulos applied two, key simplifications to obtain a much more accurate two-dimensional model, which he described as the "approximate isotropic" approach. First, from computations for the

fully three-dimensional, anisotropic cases, Lambropoulos identified that two shear components of the stress tensor in cylindrical coordinates, corresponding to $\sigma_{r\theta}$ and $\sigma_{z\theta}$, were significantly smaller than all other stress components. Noting that these results were consistent with prior analyses by Antonov *et al.* [51], he suggested that that these terms could be neglected. Next, he ignored the θ-dependence of the underlying anisotropic elastic constants, based on knowledge of prior approximate solutions for orthotropic elasticity problems by Schimke *et al.* [52]. Using these ideas, he was able to compute two-dimensional stress fields accurate to within 6% of the three-dimensional, anisotropic results. More recently, this approach has been used by Gao *et al.* [32, 53] to predict thermal stresses during silicon crystal growth without resorting to fully three-dimensional computations.

Following Gao *et al.* [32] for a system exhibiting linear elastic behavior, no plastic deformation, and linear, isotropic chemical strain, the approximate isotropic approach of Lambropoulos is written as:

$$\begin{bmatrix} \sigma_{rr} \\ \sigma_{\theta\theta} \\ \sigma_{zz} \\ \sigma_{rz} \end{bmatrix} = \begin{bmatrix} E_{11}+\lambda_{11} & E_{12}+\lambda_{12} & E_{13}+\lambda_{13} & 0 \\ E_{12}+\lambda_{12} & E_{22}+\lambda_{22} & E_{23}+\lambda_{22} & 0 \\ E_{13}+\lambda_{13} & E_{23}+\lambda_{23} & E_{33}+\lambda_{33} & 0 \\ 0 & 0 & 0 & E_{44}+\lambda_{44} \end{bmatrix} \begin{bmatrix} \epsilon_{rr}-\alpha C(r,z) \\ \epsilon_{\theta\theta}-\alpha C(r,z) \\ \epsilon_{zz}-\alpha C(r,z) \\ \epsilon_{rz} \end{bmatrix}, \tag{1}$$

where σ_{ij} are components of the stress tensor, ϵ_{ij} are components of the strain tensor, α is the chemical expansion coefficient, and $C(r,z)$ is the europium dopant concentration distribution that arises from segregation during growth. We note that Onken *et al.* [42] reported anisotropic Eu doping strain along different BaBrCl lattice directions; however, we have employed an averaged, isotropic chemical expansion coefficient, α, to simply our analysis. The coefficients E_{ij} correspond to the fundamental elastic constants of an orthorhombic crystal whose c-axis is aligned with the z-axis of a Cartesian coordinate system [11], with indices $\{1,2,3\}$ corresponding to $\{x,y,z\}$. The constants λ_{ij}, defined by Gao *et al.* [32, 53] from earlier derivations [49, 50], are included to account for anisotropies that arise due to specific crystallographic orientation and transformation to cylindrical coordinates. While Lambropoulos developed this method for computing stresses in a crystal of cubic symmetry, we assume that this approach is also reasonable for describing the vertical Bridgman growth of the orthorhombic BaBrCl crystal. While a cubic crystal has three independent elastic constants, an orthorhombic crystal has nine [11]. Seven of those independent, orthorhombic elastic coefficients are represented in eq. (1), and the other two coefficients correspond to shear terms of the three-dimensional stress tensor that are neglected in the approximate isotropic approach [50]. Thus, there is little mathematical distinction between cubic and orthorhombic symmetries in the approximation of Lambropoulos [50], and we apply this method to compute chemical stress here.

We finish the problem formulation by prescribing that there is no crystal-ampoule interaction with respect to the effects of chemical stress, yielding a traction-free condition applied along all the outer surfaces of the cylindrical domain representing the crystal in the ampoule,

$$\mathbf{n} \cdot \boldsymbol{\sigma} = \mathbf{0}, \tag{2}$$

where $\mathbf{n}$ is the vector normal to the outer surfaces and $\mathbf{0}$ denotes the null vector.

The resulting mechanics model is written as a second-order, partial differential equation for the displacement field, and a finite element method is applied for solution. We refer interested readers to the prior work of Gao and co-workers for a more complete description of the formulation and numerical solution method [29–32, 53]. The computation domain for chemical stress calculation comprises 4,096 triangular elements and is shown in Figure 1(c).

3. Results

The physical properties employed in both computational models are listed in Table 1. Estimates of properties for the growth and segregation calculation are based on our prior work [6] and on recent experiments performed at Lawrence Berkeley National Laboratory (LBNL).

The chemical stress simulations based on eq. (1) employ elastic coefficients for BaBrCl estimated from fundamental computations of $BaCl_2$ and $BaBr_2$ [54], with λ_{ij} computed for a cylindrical crystal grown in the $\langle 0\,0\,1 \rangle$ direction [49, 50]. The chemical expansion coefficient was calculated from the measurements of BaBrCl:Eu lattice constants via neutron diffraction by Onken *et al.* [42]. Europium is a substitutional dopant for barium in the BaBrCl lattice [3], and there is a local contraction when Eu, with an ionic radius of 1.30 Å, replaces Ba, with an ionic radius of 1.47 Å[55, 56]. Therefore, the chemical expansion coefficient of Eu in BaBrCl is negative.

Our approach is to first apply the transient crystal growth model to simulate an experiment performed at a constant growth rate, V_g. After enough simulated growth time has passed for the crystalline phase to fill greater than 85% of the volume of the ampoule, the model computations are terminated. Then, the Eu composition field, $C(r, z)$, predicted by the growth model is applied to the cylindrical domain of the solid mechanics model to compute the residual chemical stress in the grown crystal. Note that here we consider only chemical stresses arising from dopant distribution; we do not explicitly consider any thermally induced stresses that would be added to or subtracted from this chemical stress field at different times during growth and cool-down. In other work, this two-model coupling approach has been used to consider thermal stresses in other crystal growth systems using temperature field modeling for input to the solid mechanics model

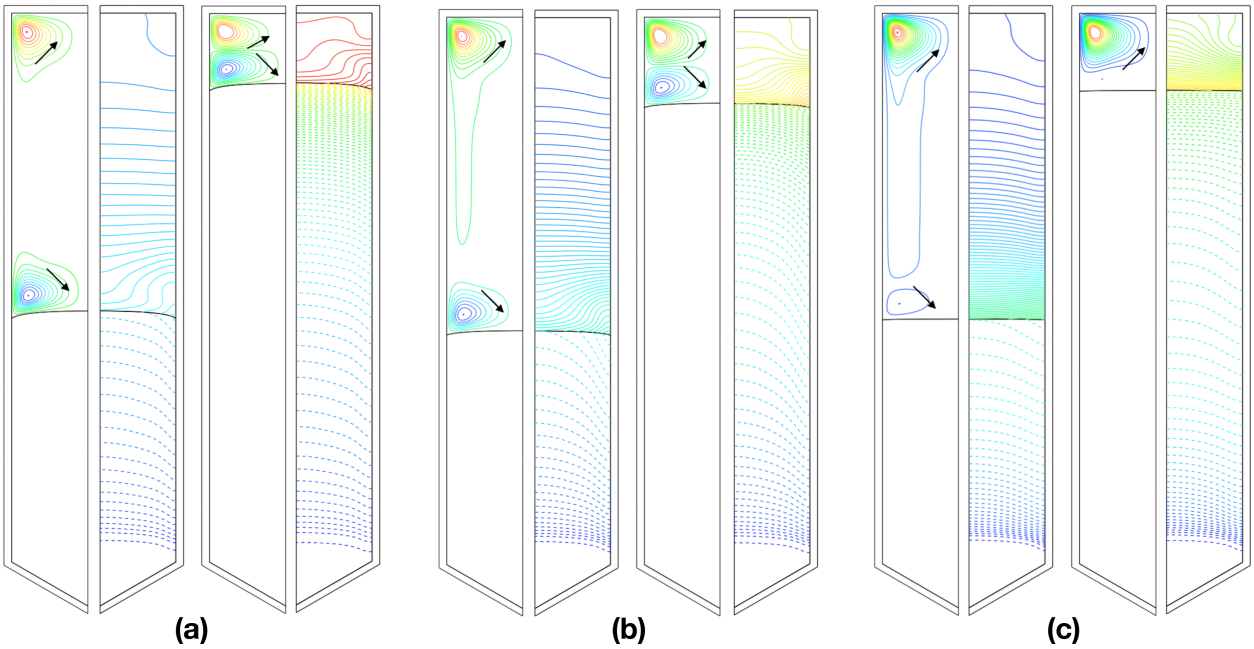

Figure 2: Snapshots of the system at two stages of growth for different growth rates, V_g. Instantaneous streamlines show flows in the melt on the left; circulation is indicated by arrows. Iso-concentration lines, with a constant spacing of 0.05 mole% Eu, are plotted on the right to show the dopant concentration field. (a) The case of $V_g = 1$ mm/hr, after 19.4 hours and 38.9 hours. (b) The case of $V_g = 2$ mm/hr, after 9.15 hours and 18.9 hours. (c) The case of $V_g = 3.2$ mm/hr, after 6.1 hours and 12.2 hours.

[29–32, 53].

3.1. Crystal growth and Eu segregation

Figure 1(a) shows the initial condition that represents a stationary ampoule in which a small crystal has already been grown. The solid-liquid interface is convex, because the solid thermal conductivity is approximately two times that of the melt and there is no generation of latent heat while the ampoule is at rest. Near the convex solid-liquid interface, the fluid at the ampoule wall is warmer than at the centerline, and buoyancy drives fluid upward along the ampoule wall and downward along the centerline, leading to a clockwise flow in the melt, as seen in the left meridional flow plane shown in the figures. There is also a counterclockwise vortex nested in the upper portion of the melt that is driven by thermal end effects. The initial Eu concentrations, not shown in Figure 1(a), are uniform at 2.5% in the solid and 5% in the melt, consistent with the doping level in our previous BaBrCl:Eu crystal growth experiments [5, 6] and the europium equilibrium distribution coefficient of $k = 0.5$.

For all of the following simulations, growth is simulated from time zero as the furnace temperature profile is immediately translated upward at a constant rate. We consider the vertical Bridgman growth of BaBrCl:Eu at five different growth rates, V_g, in the next several cases. Two instantaneous states are shown for each transient simulation—the first with the interface midway up the ampoule and the second

Table 1: Physical properties used in the simulations.

Property (units)	**Material**	**Symbol**	**Value**
Thermal Conductivity ($\mathrm{W\,m^{-1}\,K^{-1}}$)	BaBrCl melt	k_m	0.28 [57]
	BaBrCl crystal	k_s	0.55†
	Quartz ampoule	k_a	6
Heat Capacity ($\mathrm{J\,kg^{-1}\,K^{-1}}$)	BaBrCl melt	$E_{\mathrm{p},m}$	423 [58]
	BaBrCl crystal	$E_{\mathrm{p},s}$	385†
	Quartz ampoule	$E_{\mathrm{p},a}$	730
Density ($\mathrm{kg\,m^{-3}}$)	BaBrCl crystal	ρ_m	4660
	BaBrCl melt	ρ_s	4660
	Quartz Ampoule	ρ_a	2650
Dynamic Viscosity (Pa s)	BaBrCl Melt	μ	4.5×10^{-3} [59]
Eu Diffusion Coefficient ($\mathrm{m^2\,s^{-1}}$)	BaBrCl melt	$\mathcal{D}_m$	1.0×10^{-8}‡
	BaBrCl crystal	$\mathcal{D}_s$	1.0×10^{-12}*
Volumetric Thermal Expansion Coefficient ($\mathrm{K^{-1}}$)	BaBrCl Melt	β_{T}	2.23×10^{-4} [60]
Eu Distribution Coefficient	BaBrCl	k	0.5†
Latent Heat of Fusion ($\mathrm{J\,kg^{-1}\,K^{-1}}$)	BaBrCl	ΔH_f	94,000†
Melting Point (K)	BaBrCl	T_m	1153 [7]
Elastic Constants (GPa)**	BaBrCl Crystal	E_{11}	37.8
		E_{12}	18.8
		E_{13}	20.2
		E_{22}	38.1
		E_{23}	22.4
		E_{33}	53.2
		E_{44}	3.7
Chemical Expansion Coefficient ($[\text{mole }\%]^{-1}$)	Eu in BaBrCl crystal	α_{c}	-0.045 [42]

† Measured from recent experiments.

‡ Adapted from the diffusion coefficient of Eu in molten LiF-CaF_2 [61].

* Estimated.

** These values are estimated from density-functional theory (DFT) calculations of the elastic constants for $BaCl_2$ and $BaBr_2$ [54].

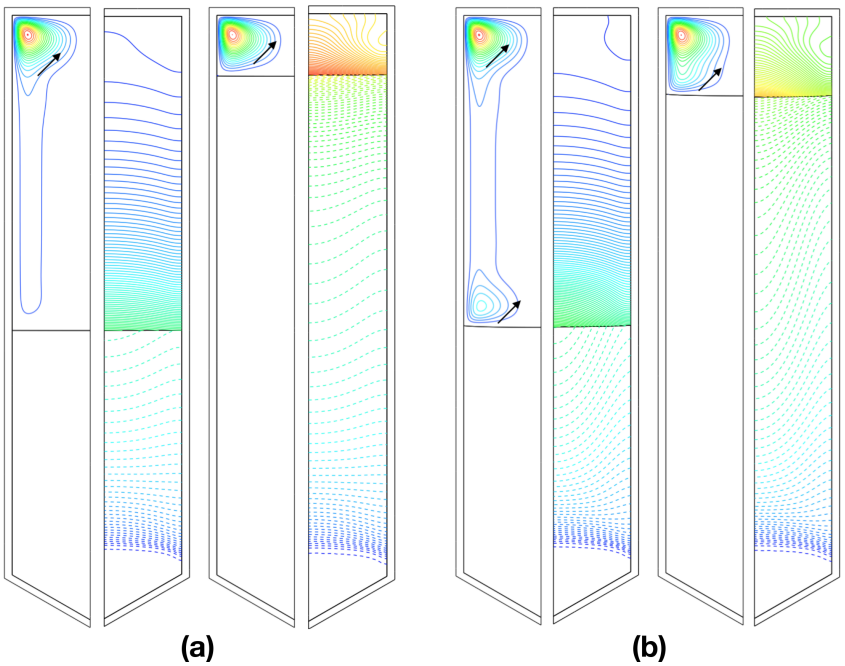

Figure 3: Snapshots of the system at two stages of growth for different growth rates, V_g. Instantaneous streamlines show flows in the melt on the left; circulation is indicated by arrows. Iso-concentration lines, with a constant spacing of 0.05 mole% Eu, are plotted on the right to show the dopant concentration field. (a) The case of $V_g = 3.5$ mm/hr, after 5.5 hours and 11.5 hours. (b) The case of $V_g = 4$ mm/hr, after 4.9 hours and 9.7 hours.

near the end of the growth run. For each state of growth, the form of the flow field in the melt is indicated via instantaneous streamlines plotted with constant spacing on the left meridional plane, and the europium distribution is shown via constantly-spaced iso-concentration contours on the right. All plots employ the same contour spacing and color scale. For reference, Bourret *et al.* [2, 4, 5, 7] typically employed growth rates of between 0.5 and 1.5 mm/hr in their experiments.

Figure 2(a) shows the case for an applied growth rate of $V_g = 1$ mm/hr. The shape of the solid-liquid interface remains convex with respect to the crystal over the entire growth run. The radial temperature gradients also remain nearly constant over time, and the buoyant flow near the interface keeps its clockwise circulation at a nearly constant strength, with a maximum velocity of $v_{max} \approx 0.035$ mm/s. In this and all following cases, melt flows are dominated by viscosity; here, a Reynolds number is computed as $Re = \rho_m v_{max} R/\mu \approx 0.21$. The flow has very little effect on heat transfer but is strong enough to interact with the diffusion layer of europium created by rejected solute along the interface during growth. The lower flow cell sweeps Eu atoms in the enriched, diffusion layer toward the ampoule wall, resulting in radial concentration profiles in the grown solid with higher Eu concentration along the outer regions and lower in the interior.

For the case of $V_g = 2$ mm/hr, the greater amount of latent heat released by faster growth produces a solid-liquid interface that is less convex than that for the $V_g = 1$ mm/hr case. Accompanying this flatter interface is a smaller radial temperature gradient, and the flow near the interface, though still clockwise, is

much weaker. However, at this faster growth rate, the diffusion layer consisting of enriched Eu is substantially thinner and more susceptible to convection by the outward radial flow along the interface. The end result is a crystal of even higher Eu concentration on the outer surface and a larger radial concentration gradient over most of its length, compared to the $V_g = 1$ mm/hr case.

An applied growth rate of $V_g = 3.2$ mm/hr is shown in Figure 2(c). At this growth rate, the latent heat release is enough to nearly flatten the shape of the solidification interface, although it is still very slightly convex with respect to the solid. Correspondingly, the temperature profile near the interface is very nearly free from radial variation, and the melt flow is very weak. Nevertheless, the clockwise flow adjacent to the interface interacts with the segegration-induced Eu diffusion layer to give rise to a moderate radial gradient for the solute in the solid. This radial gradient is in the same direction, with higher concentration near the wall, though smaller in magnitude than the two prior cases.

Figure 3(a) shows the case for a growth rate of $V_g = 3.5$ mm/hr. Here, the incrementally increased release of latent heat causes the interface to be slightly *concave* with respect to the solid. With the concave interface comes a reversal in the radial temperature profile over the previous cases, which is now warmer at the centerline than at the ampoule wall. This causes a reversal in the direction of flow along the interface, which is now flowing inward toward the centerline. This change in flow direction reverses the radial Eu profile, which results in lower solute concentrations in the outer regions of the crystal over most of its length.

The highest growth rate of $V_g = 4$ mm/hr, shown in Figure 3(b), increases the concavity of the solid-liquid interface via latent heat release, which significantly strengthens the inward flow along the interface. This strong counterclockwise flow sweeps Eu atoms in the enriched diffusion layer towards the centerline and results in significant radial concentration gradients, with higher Eu levels in the center and lower in the outer annular regions of the grown crystal.

3.2. Chemical stress and the propensity for cracking

As described previously, the Eu concentration fields computed for crystals grown under different growth rates are supplied to compute strains and stresses caused by chemical effects. We emphasize that the stresses shown here arise only from the distribution of the europium dopant throughout the crystal caused by segregation during growth. We do not consider thermally-induced stresses,; however, additional remarks on the importance and role of thermal stresses are presented in the conclusions section.

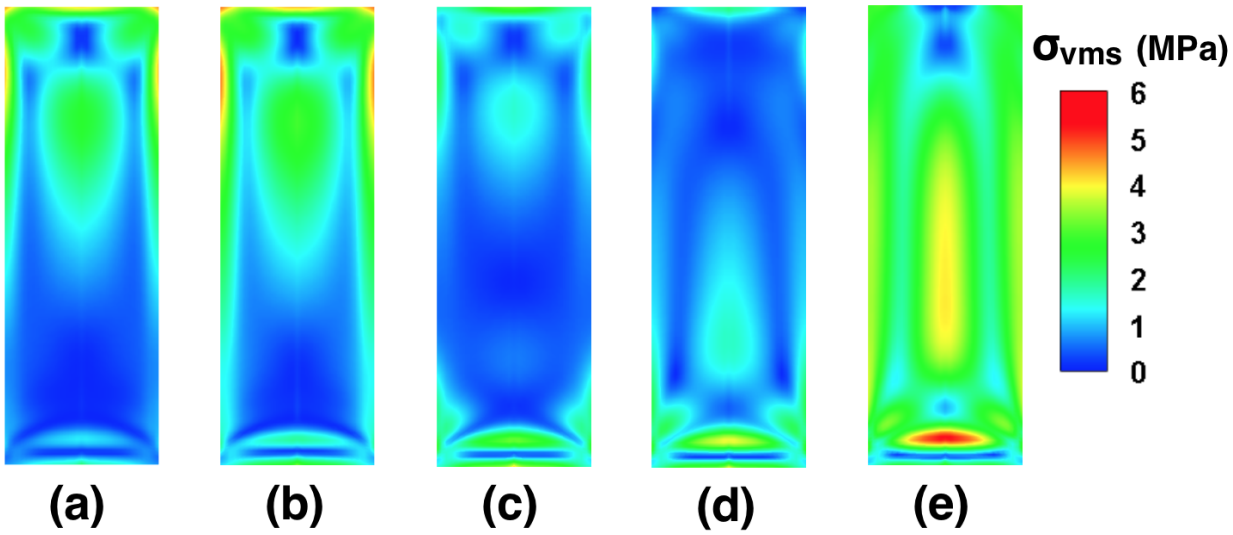

Figure 4: The von Mises stress, σ_{vms}, arising from chemical strain is shown across the entire meridional plane of the crystal for growth rates of (a) $V_g = 1$ mm/hr, (b) $V_g = 2$ mm/hr, (c) $V_g = 3.2$ mm/hr, (d) $V_g = 3.5$ mm/hr, and (e) $V_g = 4$ mm/hr.

3.2.1. Shear stresses

The von Mises stress, σ_{vms}, arising from chemical strain is plotted for each case in Figure 4. This quantity is the second invariant of the deviatoric part of the stress tensor,

$$\sigma_{vms} = \left(\frac{1}{2}[(\sigma_{rr} - \sigma_{zz})^2 + (\sigma_{zz} - \sigma_{\theta\theta})^2 + (\sigma_{\theta\theta} - \sigma_{rr})^2] + 3\sigma_{rz}^2 \right)^{1/2}, \tag{3}$$

and represents a physical measure of the shear strain energy. As a scalar quantity, the von Mises stress is a convenient indicator of the general magnitude of shear stresses within the crystal.

Apart from the bottom regions, where there are significant changes in axial europium concentration caused by the initial growth transient, there are larger variations in the von Mises stresses in the radial direction than in the axial direction for all cases. Thus, radial segregation of europium is more important than axial segregation in producing residual chemical shear stresses.

The Von Mises stress is always a positive quantity, and, while it increases with spatial variation of the europium dopant, it does not depend on the direction of the compositional gradients in the crystals. Thus, one observes that the von Misses stresses are generally larger with greater degrees of segregation and smaller for those cases with a more homogeneous distribution of europium. Reduced stress states are evident for the cases that minimize radial compositional variations, specifically those cases corresponding to $V_g = 3.2$ mm/hr and $V_g = 3.5$ mm/hr, shown in Figure 4(c) and (d), respectively. These growth states featured relatively flat interfaces and minimal radial segregation.

Very high shear stresses could potentially drive the cracking of a brittle material via sliding and tearing,

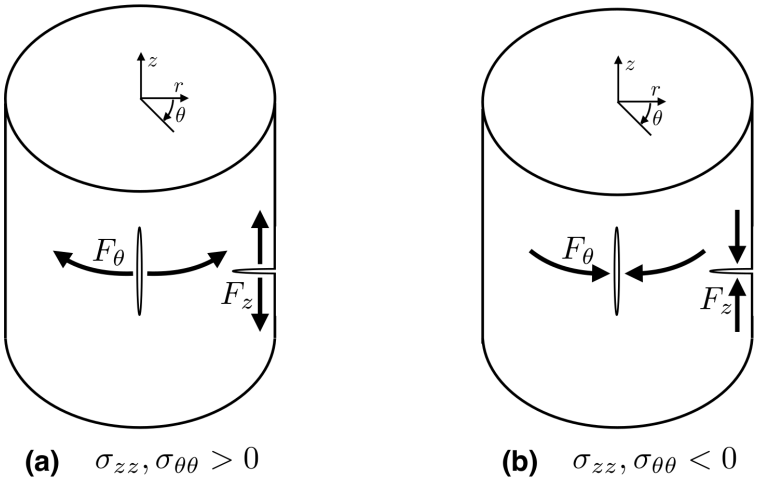

Figure 5: (a) Mode I crack opening occurs under forces produced by tensile normal stresses, corresponding to positive σ_{zz} and $\sigma_{\theta\theta}$. (B) Compressive normal stresses, with negative σ_{zz} and $\sigma_{\theta\theta}$, produce forces that suppress crack opening and propagation.

also known as mode II and mode III crack opening, respectively [62, 63]. However, we do not believe that chemical stresses from segregation are high enough to enable these mechanisms. Rather, chemical shear stresses could augment thermal stresses at high temperature to drive plastic deformation during crystal growth, thus resulting in higher residual stresses than would be present from thermal effects alone. While this could be important for some ductile materials, we have not considered such residual stresses caused by high-temperature yield in the brittle crystals considered in this study.

3.2.2. Normal stresses

Normal stresses are much more relevant in the cracking of brittle crystals, such as BaBrCl, via the mode I crack opening mechanism [62, 63], whereby normal forces act to open or close a micro-crack. This mechanism for brittle fracture was originally considered in the seminal work of Griffith [38] and is depicted schematically in Figure 5, where the resultant forces, F_z and F_θ, of normal stresses, σ_{zz} and $\sigma_{\theta\theta}$, respectively, are acting on surface imperfections. While the tensile stresses depicted in Figure 5(a) produce forces that open cracks, the compressive stresses shown in Figure 5(d) result in forces that act to close them. Note that, in this study, the σ_{rr} normal component of chemical stress is zero along the outer surface of the crystal due to the traction-free boundary condition applied there.

We show the distribution of normal stresses, σ_{zz} and $\sigma_{\theta\theta}$, for the different crystal growth cases in Figures 6 and 7, respectively. As was the case for von Mises stresses, radial changes in normal stresses are more prominent than axial variations. The most significant feature of these stress fields is the change of sign in normal stress from interior to surface. For the cases at lower growth rates, with $V_g \leq 3.2$ mm/hr, the normal stresses are compressive in the interior and tensile along most of the cylindrical outer surface of the crystal. When the growth rate exceeds this value, as in the cases shown for $V_g = 3.5$ mm/hr and $V_g = 4$ mm/hr in

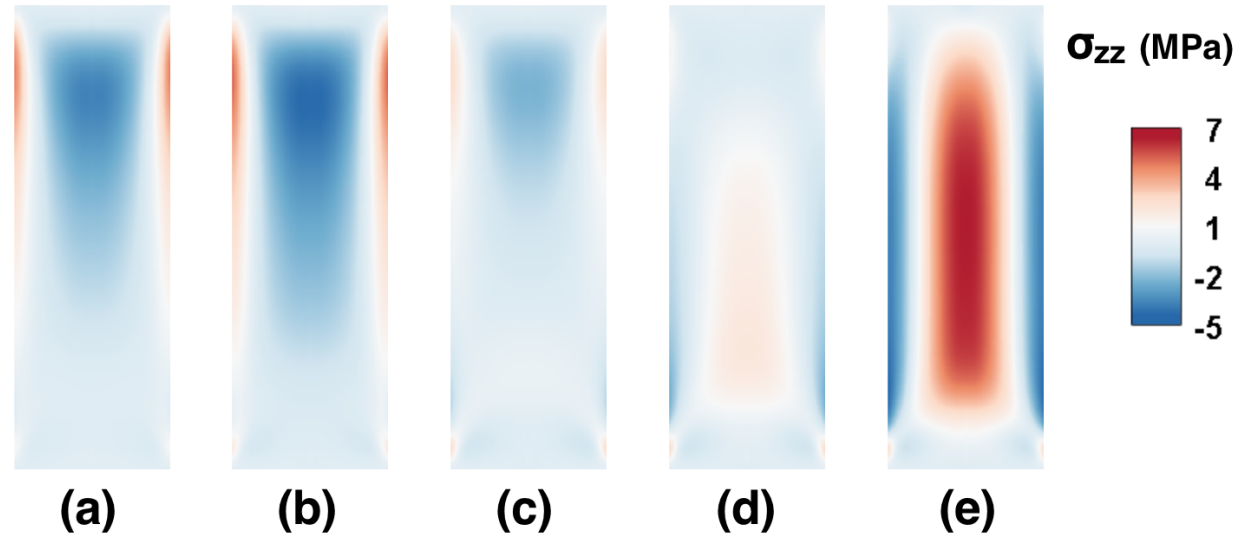

Figure 6: The component of axial normal stress, σ_{zz}, arising from chemical strain is shown across the entire meridional plane of the crystal for growth rates of (a) V_g = 1 mm/hr, (b) V_g = 2mm/hr, (c) V_g = 3.2 mm/hr, (d) V_g = 3.5 mm/hr, and (e) V_g = 4 mm/hr. Positive values are tensile and plotted in shades of red; negative values are compressive and plotted in shades of blue.

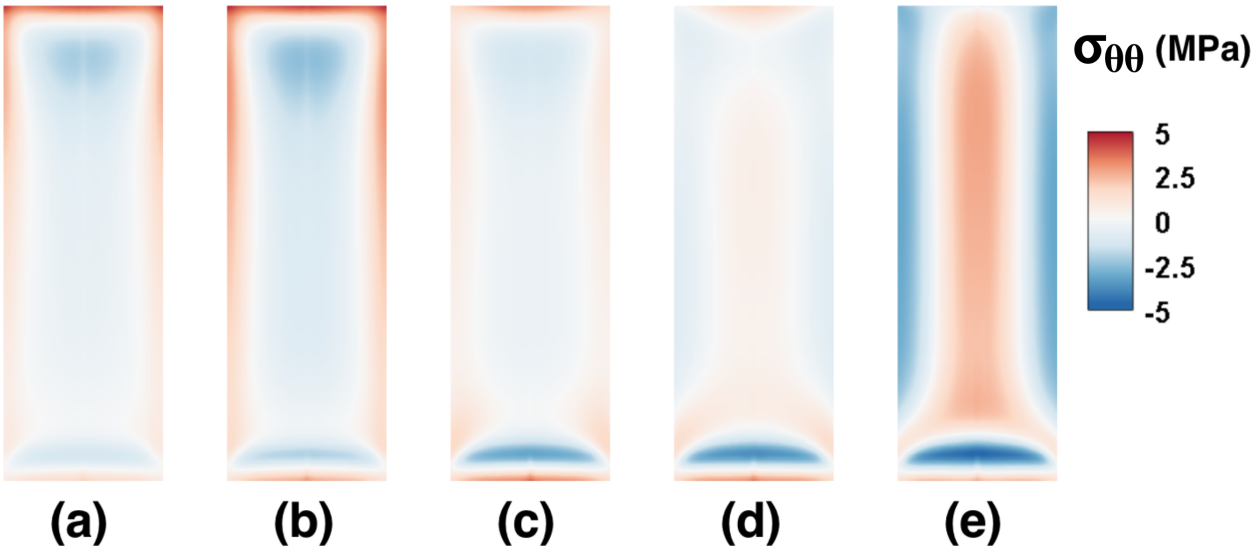

Figure 7: The component of azimuthal normal stress, $\sigma_{\theta\theta}$, arising from chemical strain is shown across the entire meridional plane of the crystal for growth rates of (a) V_g = 1 mm/hr, (b) V_g = 2 mm/hr, (c) V_g = 3.2 mm/hr, (d) V_g = 3.5 mm/hr, and (e) V_g = 4 mm/hr. Positive values are tensile and plotted in shades of red; negative values are compressive and plotted in shades of blue.

(d) and (e) of Figures 6 and 7, the distribution reverses, with tensile interior stress fields and compressive stresses along the outer surface.

Mechanistically, this reversal of the normal stress field components corresponds with a change in sign of the radial concentration gradient of europium, dC/dr. A negative radial concentration gradient, $dC/dr < 0$, such as occurs at lower growth rates and convex interface shapes, produces compressive stresses within the interior of the crystal and tensile stresses along the exterior surface. Conversely, a positive radial concen-

tration gradient, $dC/dr > 0$, reverses the stress states, with tensile stresses in the interior and compressive stresses along the outer surface.

4. Discussion

Cracking during growth and after cool down is determined by the total stress within the crystal, which is set by the sum of instantaneous thermal and residual chemical stresses.[1] In the following discussion, we comment on each of these mechanisms and their importance in the cracking of BaBrCl:Eu crystals.

Our analyses indicate that instantaneous thermal stress *during growth* is negligible compared to residual chemical stress caused by europium doping in this system [64]. However, there is evidence that thermal stress is important *after growth.* In particular, cracking of BaBrCl crystals during cool-down was reported to be problematic by Yan *et al.* [7]. Supporting these observations, Onken *et al.* [42] found that the BaBrCl coefficients of thermal expansion for the three orthorhombic crystal lattice directions are significantly different, which would likely exacerbate thermal stresses.

However, there is even stronger evidence that residual chemical stress plays a dominant role in the cracking of BaBrCl:Eu. We have observed in growth experiments that undoped BaBrCl was far less prone to cracking than Eu-doped crystals. Further, experimental observations have also indicated that interior cracks seemed to originate within the crystal from clusters in small regions with steep Eu concentration gradients [4, 5, 42]. Consistent with the combined effects of thermal and chemical sources of strain, Onken *et al.* [42] reported that cracking of BaBrCl:Eu was often observed to occur near a critical temperature of approximately 673 K during post-growth cooling, where they measured a change in anisotropy of dopant-induced, chemical strain.

Returning to the analyses presented above, we found that shear stresses arising from chemical strain, as measured by the von Misses stress field, were minimized when radial segregation was minimized. If cracking via mode II sliding and mode III tearing mechanisms were important, the shear forces driving such behavior would be mitigated by growth with nearly flat interfaces and little radial segregation. However, we have no experimental evidence that BaBrCl:Eu crystals grown under conditions that produced low radial segregation were less prone to cracking.

Rather, we believe that normal stresses arising from non-uniform europium distributions are more important for the cracking of the brittle BaBrCl host. First, normal stresses produced by chemical effects are roughly two times larger than shear stresses when radial segregation is significant. Second, experimental observation that cracking behavior changes with different growth conditions is more consistent with the

[1] Again, we are ignoring the case of residual stresses caused by plastic deformation from dislocation multiplication and movement caused by thermal shear stresses, as briefly discussed in Section 3.2.1. Such residual stresses from thermal history may be important in some crystal growth systems.

nature of the mode I crack opening mechanism that was depicted schematically in Figure 5. In particular, tensile stresses acting upon a micro-crack will open and propagate it, while compressive stresses will suppress opening and propagation. These behaviors depend upon the sign of the local normal stress and are readily changed by the dopant concentration profile. This argues that different growth conditions, particularly those impacting radial segregation, should have a significant impact on the propensity for crystal cracking.

Clearly, experimental evidence confirms that europium doping increases the likelihood for cracking of BaBrCl. However, our theoretical analyses present a compelling set of ideas that go beyond the simple correlation between Eu doping levels and cracking. The results of our analysis suggest that the *spatial distribution* of the dopant, not necessarily the doping level, is critical to determine the propensity for cracking.

At lower growth rates in this system, the interface is convex, and the flows near the interface lead to $dC/dr > 0$, which produces tensile normal stresses around the periphery of the crystal. These tensile stresses promote crack opening from surface flaws. Conditions are reversed when growth is fast enough to generate sufficient latent heat to deflect the interface into a concave shape and reverse the radial temperature gradient. The resulting inward radial flow of melt along the solid-liquid interface redistributes Eu in the growing crystal so that $dC/dr < 0$. This radial dopant profile gives rise to the outer periphery regions being under compression, which inhibits crack propagation from micro-cracks along the surface. This suggests that faster growth in this system will reduce the likelihood for cracking.

Strikingly, this strategy runs contrary to the classical wisdom that slower growth improves outcomes and that flat or slightly convex interface shapes are desirable. We also note that the overall radial europium homogeneity at these higher growth rates is comparable to that attained at lower growth rates, so scintillation performance is not compromised by faster growth in this system. Of course, there are other considerations that may limit growth at faster rates. In particular, there is always a trade-off between growth rate and interface stability in doped systems due to the possibility of interfacial instability via constitutional supercooling [65–68]. In addition, avoiding constitutional supercooling at higher growth rates via the application of larger axial thermal gradients will increase thermal stresses during growth.

Finally, the idea to tailor compressive surface stresses to inhibit cracking is not new. It has long been known that glass sheets may be immersed in ion-exchange baths to alter chemistry in a manner that induces compressive surface states, thus inhibiting cracking and adding strength [69–72]. These processing techniques have proven quite beneficial to produce thin, tough glass plates for applications such as electronic touch screens [73].

5. Conclusions

In this study, we have presented computational modeling of continuum transport, phase transformation, and chemical residual stress using coupled crystal growth and continuum mechanics models for the vertical Bridgman growth of BaBrCl doped with Eu. Our results show that significant levels of chemical stress are caused by the segregation of europium during growth. Axial segregation does not have a strong effect on stress levels, rather the more important factor is the radial compositional profile across the crystal. Of further significance is that the chemical strain distribution is determined by the sign of the radial concentration gradient and that different radial dopant profiles can either lead to *tensile* surface stress fields that enhance crack opening or *compressive* surface stresses that suppress it.

Paradoxically, faster growth rates promoted the reversal of radial flows near the interface, producing chemical strain leading to favorable compressive surface stresses in this growth system. Other approaches could be employed to the same end, such as engineering the desired radial thermal gradient and melt flows via a different furnace temperature profile [74]. We note also that, for dopants with a distribution coefficient less than unity or those introducing a positive chemical strain when incorporated into the lattice, the growth strategies that produce compressive surface stresses would be different than those discussed here.

More broadly, our analysis suggests an alluring idea—that a favorable residual chemical stress field could be tailored via dopant segregation to provide a counter-measure to cracking promoted by underlying thermal stresses. This is particularly significant, because strategies to reduce thermal stress are likely to decrease process output. For example, temperature gradients can be reduced to decrease instantaneous thermal stress during growth, but these new thermal conditions may require a slower growth rate to avoid instability of the solid-liquid interface via constitutional supercooling. After growth, thermal stresses are reduced by extending the period of cool-down, but at the expense of longer process times. In contrast, a protective chemical residual stress field could decrease high states of stress and reduce cracking without such productivity losses. Computational models, such as those employed here, will be invaluable toward designing segregation-induced, chemical stresses in future crystal growth processes to reduce the likelihood of cracking and improve process yields.

Acknowledgments

This work was supported in part by the funding of project LB15-ML-GammaDetMater-PD3Jf by the U.S. Department of Energy/NNSA/DNN R&D, under Awards DE-AC02-05CH11231 (managed by Lawrence Berkeley National Laboratory) and DE-NA0002514; no official endorsement should be inferred. We would

like to acknowledge A. Yeckel for technical assistance with the Cats2D code and D. Poerschke for useful discussion on the effects of the Eu ionic radius to produce local strain.

References

[1] J. Selling, M. Birowosuto, P. Dorenbos, S. Schweizer, Europium-doped barium halide scintillators for x-ray and γ-ray detections, Journal of Applied Physics 101 (2007) 034901.

[2] E. D. Bourret-Courchesne, G. A. Bizarri, G. R. Borade, R., E. C. Samulon, Z. Yan, S. E. Derenzo, Crystal growth and characterization of alkali-earth halide scintillators, Journal of Crystal Growth 352 (1) (2012) 78–83.

[3] G. Gundiah, Z. Yan, G. Bizarri, S. E. Derenzo, E. D. Bourret-Courchesne, Structure and scintillation of Eu^{2+}-activated BaBrCl and solid solutions in the $BaCl_2$–$BaBr_2$ system, J. Luminescence 138 (2013) 143–149.

[4] A. S. Tremsin, M. G. Makowska, D. Perrodin, T. Shalapska, I. V. Khodyuk, P. Trtik, P. Boillat, S. C. Vogel, A. S. Losko, M. Strobl, L. T. Kuhna, G. A. Bizarri, E. D. Bourret-Courchesne, *In situ* diagnostics of the crystal-growth process through neutron imaging: Application to scintillators, Journal of Applied Crystallography 49 (2016) 743–755.

[5] A. S. Tremsin, D. Perrodin, A. S. Losko, S. C. Vogel, M. A. M. Bourke, G. A. Bizarri, E. D. Bourret-Courchesne, Real-time crystal growth visualization and quantification by energy-resolved neutron imaging, Sci. Reports 7 (46275) (2017) 1–9.

[6] J. J. Derby, C. Zhang, J. Seebeck, J. H. Peterson, A. S. Tremsin, D. Perrodin, G. A. Bizarri, E. D. Bourret, A. S. Losko, S. C. Vogel, Computational modeling and neutron imaging to understand interface shape and solute segregation during the vertical gradient freeze growth of BaBrCl:Eu, Journal of Crystal Growth (2020) in press.

[7] Z. Yan, T. Shalapska, E. D. Bourret, Czochralski growth of the mixed halides BaBrCl and BaBrCl:Eu, Journal of Crystal Growth 435 (2016) 42–45.

[8] K. O. Findley, J. Johnson, D. F. Bahr, F. P. Doty, J. Frey, Fracture and deformation behavior of common and novel scintillating single crystals, in: F. P. Doty, H. B. Barber, H. Roehrig (Eds.), Penetrating Radiation Systems and Applications VIII, Vol. 6707, International Society for Optics and Photonics, SPIE, 2007, pp. 57 – 68.

[9] J. C. Brice, The cracking of Czochralski-grown crystals, J. Crystal Growth 42 (1977) 427–430.

[10] N. Miyazaki, H. Uchida, T. Tsukada, T. Fukuda, Quantitative assessment for cracking in oxide bulk single crystals during Czochralski growth: development of a computer program for thermal stress analysis, Journal of Crystal Growth 162 (1) (1996) 83 – 88.

[11] N. Miyazaki, Development of a thermal stress analysis system for anisotropic single crystal growth, Journal of Crystal Growth 236 (1) (2002) 455 – 465.

[12] H. Zhang, L. Zheng, H. Fang, Hot zone design for controlled growth to mitigate cracking in laser crystal growth, Journal of Crystal Growth 318 (1) (2011) 695 – 699.

[13] N. Miyazaki, Thermal stress and dislocations in bulk crystal growth, in: T. Nishinaga, P. Rudolph (Eds.), Handbook of Crystal Growth, 2nd Edition, Vol. II, Part A, Elsevier, 2015, Ch. 26, pp. 1049–1092.

[14] A. Ballman, J. Carruthers, H. O'Bryan, Growth of uncracked barium-sodium niobate crystals, Journal of Crystal Growth 6 (2) (1970) 184 – 186.

[15] B. Cockayne, B. Lent, J. S. Abell, I. R. Harris, Cracking in yttrium orthoaluminate single crystals, J. Mater. Sci. 8 (1973) 871–875.

[16] D. Eakins, M. Held, M. Norton, D. Bahr, A study of fracture and defects in single crystal YAG, Journal of Crystal Growth 267 (3) (2004) 502 – 509.

[17] T. Utsu, S. Akiyama, Growth and applications of Gd_2SiO_5:Ce scintillators, Journal of Crystal Growth 109 (1) (1991) 385 – 391.

[18] N. Miyazaki, A. Hattori, H. Uchida, Thermal shock cracking of lithium niobate single crystal, J. Mater. Sci. 8 (1997) 133–138.

[19] K. Y. N. Miyazaki, T. Tamura, Cracking of GSO single crystal induced by thermal stress, Computer Modeling in Engineering & Sciences 1 (1) (2000) 99–106.

[20] S. Sabharwal, Sangeeta, Investigations on cracking in $CdWO_4$ crystals, Journal of Crystal Growth 216 (1) (2000) 535 – 537.

[21] J. Johnson, K. O. Findley, F. P. Doty, The deformation and fracture behavior of the scintillating crystal cadmium tungstate, JOM 60 (4) (2008) 56–58.

[22] A. Lindsey, W. McAlexander, L. Stand, Y. Wu, M. Zhuravleva, C.L.Melcher, Crystal growth and spectroscopic performance of large crystalline boules of $CsCaI_3$:Eu scintillator, Journal of Crystal Growth 427 (2015) 42–47.

[23] L. Stand, M. Zhuravleva, J. Johnson, M. Koschan, Y. Wu, S. Donnald, K. Vaigneur, E. Lukosi, C. Melcher, Exploring growth conditions and Eu^{2+} concentration effects for KSr_2I_5:Eu scintillator crystals II: ⌀ 25 mm crystals, Journal of Crystal Growth 483 (2018) 301–307.

[24] I. C. Noyan, J. B. Cohen, Residual stress: Measurement by diffraction and interpretation, Springer, 2013.

[25] J. Völkl, G. Müller, A new model for the calculation of dislocation formation in semiconductor melt growth by taking into account the dynamics of plastic deformation, Journal of Crystal Growth 97 (1) (1989) 136 – 145.

[26] C. Tsai, O. Dillon, R. J. D. A. Jr., The constitutive equation for silicon and its use in crystal growth modeling, Journal of Engineering Materials and Technology 112 (1990) 183.

[27] D. Maroudas, R. A. Brown, On the prediction of dislocation formation in semiconductor crystals grown from the melt: Analysis of the Haasen model for plastic deformation dynamics, Journal of Crystal Growth 108 (1) (1991) 399 – 415.

[28] H. Klapper, P. Rudolph, Defect generation and interaction during crystal growth, in: T. Nishinaga, P. Rudolph (Eds.), Handbook of Crystal Growth, 2nd Edition, Elsevier, 2015, pp. 1093–1142.

[29] B. Gao, K. Kakimoto, Three-dimensional analysis of dislocation multiplication in single-crystal silicon under accurate control of cooling history of temperature, Journal of Crystal Growth 396 (2014) 7–13.

[30] B. Gao, S. Nakano, N. Miyazaki, K. Kakimoto, Alexander-Haasen model of basal plane dislocations in single-crystal sapphire, Crystal Growth and Design 14 (2014) 4080–4086.

[31] B. Gao, K. Jiptner, S. Nakano, H. Harada, Y. Miyamura, T. Sekiguchi, K. Kakimoto, Applicability of the three-dimensional Alexander-Haasen model for the analysis of dislocation distributions in single-crystal silicon, Journal of Crystal Growth 411 (2015) 49–55.

[32] B. Gao, S. Nakano, H. Harada, Y. Miyamura, K. Kakimoto, Three-dimensional analysis of dislocation multiplication during thermal process of grown silicon with different orientations, Journal of Crystal Growth 474 (2017) 121–129.

[33] K. J. Bachmann, F. A. Thiel, H. Schreiber, Melt and solution growth of bulk single crystals of quaternary III-V alloys, Prog. Crystal Growth and Charact. 2 (1979) 171–206.

[34] P. Dutta, A. Ostrogorsky, Suppression of cracks in $In_xGa_{1-x}Sb$ crystals through forced convection in the melt, Journal of Crystal Growth 194 (1) (1998) 1–7.

[35] H. Kimura, H. Maeda, M. Sato, Czochrlaski growth of $Gd_3(Ga_{1-x}Al_x)_5O_{12}$ single crystals, Journal of Crystal Growth 74 (1986) 187–190.

[36] Sangeeta, D. Desai, A. Singh, M. Tyagi, S. Sabharwal, Non-stoichiometry-induced cracking in $PbMoO_4$ crystals, Journal of Crystal Growth 296 (1) (2006) 81 – 85.

[37] Sangeeta, S. Sabharwal, Role of non-stoichiometry in the cracking of oxide crystals, Journal of Crystal Growth 310 (11) (2008) 2899 – 2905.

[38] A. A. Griffith, VI. The phenomena of rupture and flow in solids, Philosophical Transactions of the Royal Society of London. Series A 221 (1921) 163–198.

[39] S. A. Hodorowicz, E. K. Hodorowicz, H. A. Elck, Preparation and characterization of the system $BaBr_xCl_{2-x}$: The structure of BaBrCl, Journal of Solid State Chemistry 48 (3) (1983) 351–356.

[40] H. A. Eick, E. Prince, A neutron diffraction and electron microscopy examination of barium bromide–barium chloride (2/1), Acta Crystallographica, Section C: Crystal Structure Communications 42 (7) (1986) 915–917.

[41] A. S. Tremsin, D. Perrodin, A. S. Losko, S. C. Vogel, M. A. M. Burke, J. H. Peterson, J. J. Derby, T. Shinohara, G. A. Bizarri, E. D. Bourret-Courchesne, *In-situ* diagnostics of scintillator crystal growth by energy-resolved neutron imaging, in: The 21st American Conference on Crystal Growth and Epitaxy, 2017.

[42] D. R. Onken, R. T. Williams, D. Perrodin, T. Shalapska, E. D. Bourret, A. S. Tremsin, S. C. Vogel, Crystal structure evolution of BaBrCl and BaBrCl:5% Eu up to 1073 K by neutron diffraction, Journal of Applied Crystallography 51 (2) (2018) 498–504.

[43] J. J. Derby, Macroscopic transport processes during the growth of single crystals from the melt, in: J. van der Eerden, O. Bruinsma (Eds.), Science and Technology of Crystal Growth, Kluwer Academic Publishers, Dordecht, The Netherlands, 1995, pp. 97–110.

[44] A. Yeckel, J. J. Derby, Computational simulations of the growth of crystals from liquids, in: H. Scheel, T. Fukuda (Eds.), Crystal Growth Technology, John Wiley & Sons, West Sussex, UK, 2003, Ch. 6, pp. 115–137.

[45] A. Yeckel, J. J. Derby, Computer modelling of bulk crystal growth, in: P. Capper, A. Willougby, S. Kasap (Eds.), Bulk Crystal Growth of Electronic, Optical, and Optoelectronic Materials, John Wiley & Sons, West Sussex, UK, 2005, pp. 73–119.

[46] J. J. Derby, A. Yeckel, Heat transfer analysis and design for bulk crystal growth: Perspectives on the Bridgman method, in: T. Nishinaga, P. Rudolph (Eds.), Handbook of Crystal Growth, 2nd Edition, Vol. II, Part A, Elsevier, 2015, Ch. 20, pp. 793–843.

[47] J. J. Derby, Fluid dynamics in crystal growth: The good, the bad, and the ugly, Progress in Crystal Growth and Characterization of Materials 62 (2016) 286–301.

[48] A. Yeckel, R. T. Goodwin, Cats2D (crystallization and Transport Simulator), User Manual, unpublished (http://www.cats2d.com) (2003).

[49] N. Miyazaki, S. Hagihara, T. Munakata, Elastic constant matrix required for thermal stress analysis of bulk single crystals during Czochralski growth, Journal of Crystal Growth 106 (1996) 149–156.

[50] J. C. Lambropoulos, The isotropic assumption during the Czochralski growth of single semiconductors crystals, Journal of Crystal Growth 84 (3) (1987) 349 – 358.

[51] P. I. Antonov, S. I. Bakholdin, E. V. .Galaktionov, E. A. Tropp, Izv. Akad. Nauk SSSR, Ser. Fiz. 44 (1980) 256.

[52] J. Schimke, K. Thomas, J. Garrison, Approximate solution of plane orthotropic elasticity problems, Management Information Services, Detroit, Michigan (1968).

[53] B. Gao, S. Nakano, H. Harada, Y. Miyamura, T. Sekiguchi, K. Kakimoto, Anisotropic thermal stress simulation with complex crystal-melt interface evolution for seeded growth of monocrystalline silicon, Crystal Growth and Design 12 (2012) 5708–5714.

[54] P. Kumar, A. Vedeshwar, DFT calculations of structural, electronic, optical and elastic properties of scintillator materials $BaCl_2$ and $BaBr_2$, J. Phys. D. Appl. Phys. 48 (2015) 105301.

[55] R. D. Shannon, C. T. Prewitt, Effective ionic radii in oxides and fluorides, Acta Cryst. B25 (1969) 925–946.

[56] R. D. Shannon, Revised effective ionic radii in sytematic studies of interatomic distances in halides and chalcogenides, Acta Cryst. A32 (1976) 751–767.

[57] A. Gheribi, J. Torres, P. Chartrand, Recommended values for the thermal conductivity of molten salts between the melting and boiling points, Solar Energy Materials & Solar Cells 126 (2014) 11–25.

[58] J. M.W. Chase, NIST-JANAF Thermalchemical Tables, Fourth Edition, Journal of Physical and Chemical Reference Data, Monograph 9 (Part I and Part II) (1998) 1963.

[59] G. J. Janz, R. P. T. Tomkins, C. B. Allen, J. J. R. Downey, G. L. Gardner, U. Krebs, S. K. Singer, Molten salts: Chlorides and mixtures, electrical conductance, density, viscosity, and surface tension data, Journal of Physical and Chemical Reference Data 4 (2).

[60] G. Janz, Thermal dynamic and transport properties of molten salts: Correlation equations for critically evaluated density, surface tension, electric conductance, and viscosity data, Journal of Physical and Chemical Reference Data 17 (2).

[61] L. Massot, P. Chamelot, L. Cassayre, P. Taxil, Electrochemical study of the Eu(III)/Eu(II) system in molten fluoride media, Electrochimita Acta 54 (2009) 6361–6366.

[62] M. Janssen, J. Zuidema, R. Wanhill, Fracture Mechanics : Fundamentals and Applications, 2nd Edition, CRC Press LLC, 2004.

[63] N. Perez, Fracture Mechanics, Springer, 2017.

[64] C. Zhang, Computational modeling for the growth of BaBrCl:Eu crystal, Ph.D. thesis, University of Minnesota (2020).

[65] W. A. Tiller, K. A. Jackson, J. W. Rutter, B. Chalmers, The redistribution of solute atoms during the solidification of metals, Acta Metallurgica 1 (1953) 428.

[66] W. W. Mullins, R. F. Sekerka, Stability of a planar interface during solidification of a dilute binary alloy, J. Appl. Phys. 35 (1964) 444–451.

[67] R. F. Sekerka, Morphological stability, J. Crystal Growth 3 (1968) 71.

[68] M. C. Flemings, Solidification Processes, McGraw-Hill, Inc., New York, 1974.

[69] M. E. Nordberg, E. Mochel, H. M. Garfinkel, J. S. Olcott, Strengthening by ion exchange, Journal of the American Ceramics Scociety 47 (1964) 215–219.

[70] A. Y. Sane, A. R. Cooper, Anomalous stress profiles in ion-exchanged glass, Journal of the American Ceramics Scociety 61 (1977) 359–362.

[71] A. Varshneya, Chemical strengthening of glass: Lessons learned and yet to be learned, International Journal of Applied Glass Science 1 (2) (2010) 131–142.

[72] A. Tandia, K. Vargheese, J. Mauro, A. Varshneya, Atomistic understanding of the network dilation anomaly in ion-exchanged glass, Journal of Non-Crystalline Solids 358 (2012) 316–320.

[73] D. Pogue, Gorilla Glass, the Smartphone's Unsung Hero, The New York Times.

[74] J. H. Peterson, J. J. Derby, An axial temperature profile curvature criterion for the engineering of convex crystal growth interfaces in Bridgman systems, J. Crystal Growth 468 (2017) 899–904.